Ground mobile observation system for measuring multisurface microwave emissivity

He Wenying[1,2]   Chen Hongbin[1,2]   Xuan Yuejian[1]   Lijun[1]

Nan Weidong[1, 3]   Duan Minzheng[1,2]

1.Key Laboratory of Middle Atmosphere and Global Environment Observation, Institute of Atmospheric Physics, Chinese Academy of Sciences, Beijing 100029, China

2.University of Chinese Academy of Sciences, Beijing 100049, China

3 Xianghe Observatory of Whole Atmosphere, Institute of Atmospheric Physics, Chinese Academy of Sciences, Xianghe 065400, China

Abstract

Large microwave surface emissivities with a highly heterogeneous distribution and the relatively small hydrometeor signal over land make it challenging to use satellite microwave data to retrieve precipitation and to be assimilated into numerical models. To better understand the microwave emissivity over land surfaces, we designed and established a ground observation system for the in situ observation of microwave emissivities over several typical surfaces. The major components of the system include a dual-frequency polarized ground microwave radiometer, a mobile observation platform, and auxiliary sensors to measure the surface temperature and soil temperature and moisture; moreover, observation fields are designed comprising five different land surfaces.

Based on the observed data from the mobile system, we preliminarily investigated the variations in the surface microwave emissivity over different land surfaces. The results show that the horizontally polarized emissivity is more sensitive to land surface variability than is the vertically polarized emissivity: the former decreases to 0.75 over cement and increases to 0.90 over sand and bare soil and up to 0.97 over grass. The corresponding emissivity polarization difference is obvious over water

27   (>0.3) and cement (approximately 0.25) but reduces to 0.1 over sand and 0.05 over

28   bare soil and almost 0.01 or close to zero over grass; this trend is similar to that of the

29   Tb polarization difference. At different elevation angles, the horizontally/vertically

30   polarized emissivities over land surfaces obviously increase/slightly decrease with

31   increasing elevation angles but exhibit the opposite trend over water.

32   Key words: Ground mobile observation system, microwave radiometer, microwave surface

33   emissivity, surface temperature, land surface

34   **1 Introduction**

35   The land surface microwave emissivity varies but is generally high (~ 0.90) and

36   thus generates strong surface radiance; however, this strong surface radiance obscures

37   radiance from the atmosphere and hydrometeors, making it more difficult to

38   assimilate and precisely retrieve atmospheric parameters using satellite microwave

39   data over land (McNally et al., 2000; Farbou et al., 2005; Schwartz et al., 2012).

40   Moreover, due to complex variations affected by many surface factors, such as soil

41   type, wetness, vegetation type and surface roughness, the land surface emissivity is

42   poorly understood. Hence, the land surface microwave emissivity constitutes a major

43   parameter limiting the application of spaceborne microwave data over land.

44   Microwave emissivity models have been developed only for a limited range of

45   frequencies and surface conditions. For example, the emissivity over bare soil was

46   modeled at lower frequencies, and the soil dielectric constants were obtained from

47   ground-based measurements (Wang and Schmugge, 1980). The emissivity over the

48   vegetation canopy was simulated using a radiative transfer model with a large number

49   of canopy optical parameters (Mo and Schmugge, 1987; Isaacs et al., 1989; Fung,

50   1994). Weng (2001) developed a microwave land emissivity model to quantify the

51   emissivity over various surface conditions, including snow, deserts, and vegetation.

52   Xie et al. (2017) developed a parameterized soil surface emissivity model for bare soil

53   surfaces and compared with Weng's model, results reflected the reduced overall

54   errors, especially for horizontal polarization. Ultimately, the microwave emissivity of

55   land surfaces is determined mainly by the soil dielectric constant, which is influenced

56   by the physical temperature, soil texture and moisture content, and vegetation

57   structure and type. As a result of these complicated parameters with numerous

58   uncertainties, establishing a common physical emissivity model and accurately

59   obtaining emissivity estimates by using only an emissivity model remain challenging.

60   Satellite observations offering extensive coverage have been used to estimate the

61   regional and global distributions of land surface emissivity since the 1990s (Prigent et

62   al., 2000; Moncet et al., 2011). To avoid the impacts of the complex variability of

63   clouds and precipitation in the atmosphere, only the brightness temperatures observed

64   by spaceborne microwave instruments under clear sky conditions are generally

65   selected to calculate the land surface microwave emissivity. Jones and Vonder Haar

66   (1997) used SSM/I (Special Sensor Microwave Imager) microwave observations and

67   GOES/VISSR (Geostationary Operational Environmental Satellite/Visible Infrared

68   Spin-Scan Radiometer) infrared data that were closely matched in both space and time

69   to retrieve the microwave land emissivity over the Central United States and utilized

70   the infrared data with a constant infrared emissivity of 0.98 to calculate the land skin

71 temperature (LST) under clear sky conditions. Further, Ruston and Vonder Haar (2004)

72 directly employed spatially varying infrared surface emissivities in the retrieval of

73 LST to calculate the microwave emissivity and discovered that the

74 atmospheric-corrected microwave surface emissivity is valuable for determining land

75 surface characteristics but is sensitive to rain events. Prigent et al. (1997, 1999)

76 calculated the land surface microwave emissivity over Africa, some parts of Europe

77 and West Asia by combining SSM/I data with LST observations provided by ISCCP

78 (International Satellite Cloud Climatology Project). With subsequently improved

79 ISCCP LST and cloud product data, Prigent et al. (2006) presented a global land

80 surface microwave emissivity database retrieved from 10 years of SSM/I data and

81 plotted the monthly average land surface microwave emissivity onto a geographic

82 map. In their work, the microwave emissivity retrieval was based primarily on

83 radiative transfer calculations, in which infrared data were used to determine the LST

84 under clear sky conditions, and atmospheric sounding data were used to take the

85 effects of atmospheric attenuation into account. Nevertheless, due to the complexity

86 and variability of clouds and atmospheric precipitation, land surface microwave

87 emissivity estimates derived from satellite observations are available only under clear

88 sky conditions. Moreover, the cloud screening and LST retrieval methods still contain

89 numerous uncertainties, which represent the main sources of errors in emissivity

90 calculations.

91   At present, the accuracy of surface emissivity estimates calculated from either

92 emissivity models or satellite observations is limited by the complexity of the land

93 surface and the variability of vegetation types and soil moisture. Another important

94 limitation is availability and accuracy of necessary input parameters on a global scale.

95 Hence, surface emissivity calculations need to be verified and improved with more in

96 situ observation data.

97 To better understand the variation characteristics of surface emissivity with

98 surface conditions, Ulaby et al. (1985) combined field experiments and theoretical

99 research and revealed that the land surface microwave specific emissivity is strongly

100 correlated with the distributions of soil moisture and vegetation. In addition, a few

101 observation experiments using ground-based microwave radiometers have been

102 carried out since the 1990s to study the variation characteristics of emissivity over

103 different surfaces (Njoku and O'Neill,1982; Matzler, 1990, 1994; Calvet, 1997;

104 Wigneron, 1994; Morland et al., 1995). More recently, in situ passive microwave

105 radiometer measurements over snow cover and sub-Arctic frozen soil have been used

106 to validate empirical emission models (Lemmetyinen et al., 2015; Montpetit et al.,

107 2018). Additionally, an aircraft-flown microwave radiometer was used to directly

108 observe the surface emissivity over forests, crops, snow and ice to analyze the

109 sensitivity of those emissivities to the view angle, frequency, measurement time and

110 surface characteristics (Hewison, 2001; Wigneron et al., 1997; Hewison and English,

111 1999).

112 The observation mode of a microwave radiometer in a field experiment is an

113 important consideration. Usually, ground-based radiometers are fixed when scanning

114 the observed field; for example, they can be mounted on a truck or a tower (Matzler,

115   1990; Lemmetyinen et al., 2015), allowing the instrument to better determine the

116   temporal evolution of surface emissivity over single type of land-cover area. In

117   contrast, using a mobile mode, such as airborne and mobile sled-based radiometers

118   (Morland, 2003; Lemmetyinen et al., 2015; Montpetit et al., 2018), can better reveal

119   the spatial evolution of surface emissivity over different land-cover areas, but it is not

120   easy to obtain long-term emissivity observations due to the high cost and effort.

121   To obtain the long-term temporal evolution of surface emissivity over different

122   types of surfaces simultaneously, we proposed and developed a ground mobile

123   observation system to enhance in situ microwave emissivity observations. Long-term

124   continuous emissivity field experiments can help to more accurately understand the

125   characteristics of passive microwave polarized emissivities over typical land surfaces,

126   form a benchmark for verifying the retrieved emissivities from satellite or emission

127   models, and establish an emissivity parameterization scheme for a given surface in

128   radiance assimilation. The outline of this paper is as follows: the design of the ground

129   mobile observation system for measuring surface emissivity is introduced in section 2;

130   the data and method used for the emissivity calculations are described in section 3;

131   then, the surface emissivity estimates obtained directly from the observation system

132   are discussed preliminarily in section 4; and a final short summary is given in section

133   5.

134   **2. Ground mobile observation system for surface microwave emissivity**

135   To obtain the surface emissivity over several typical surfaces simultaneously, we

136   designed a ground mobile observation system to carry out long-term field experiments

over 5 test plots. Fig. 1 is an on-site photo of the observation system operating at the

Xianghe observation site (116.98°E, 39.76°N), Hebei Province, China. As shown in

Fig. 1, the mobile observation system consists of five main parts: a dual-frequency

(18.7 and 36.5 GHz),dual-polarized ground-based microwave radiometer to observe

the surface and sky radiances, a mobile platform to move back and forth along a track,

and three auxiliary sensors to measure the surface temperature, soil temperature and

moisture. The observation field includes five test plots, namely, water, cement, sand,

bare soil and grass. From the observation system, we can directly obtain surface

microwave emissivity estimates more accurately than is possible from satellite data or

emissivity models, which is important to properly understand the variation

characteristics of land microwave emissivities and to improve the emissivity

parameterization schemes used in models.

Fig 1 On-site photo of the surface microwave emissivity observation system
operating over various surfaces at the Xianghe site, China

2.1 Ground-based microwave radiometer

154 The core device of the observation system is a dual-frequency (18.7 and 36.5

155 GHz), dual-polarized (horizontal and vertical) microwave radiometer (RPG-4CH-DP)

156 produced by Radiometer Physics GmbH, Germany. The RPG-4CH-DP radiometer is a

157 high-performance instrument with a direct detection receiver and a completely

158 automatic calibration system. The radiometer is mounted on an accurate

159 elevation/azimuth positioner so that the whole system can perform scans in any

160 direction from the sky to the ground, thereby realizing complex scanning schemes,

161 such as all-sky monitoring and all-round monitoring of the ground. The RPG-4CH-DP

162 can distinguish cloud/raindrop particles during precipitation and monitor soil moisture

163 and vegetation parameters by using signals with different polarizations. Both

164 frequencies of 18.7 GHz and 36.5 GHz have been widely combined to detect snow

165 depth and snow water content and are frequently used in most spaceborne microwave

166 imagers, such as the SSM/I, AMSR-E (Advanced Microwave Scanning Radiometer

167 for EOS) and GMI (GPM Microwave Imager) sensors. The directly observed surface

168 emissivities at these two frequencies can provide highly accurate references for the

169 verification and assimilation of spaceborne microwave observations.

170 The RPG-4CH-DP radiometer has a comparable half-power beam width of

171 approximately 6° and a calibration accuracy of ±1 K. Currently, the height of the

172 instrument above the ground is 2.5 m, which results in a half-power footprint width of

173 0.22 m on average. More details regarding the instrument specifications for the

174 RPG-4CH-DP are shown in Table 1.

175

Table 1 Instrument Specifications

Parameter	Specification
Radiometric resolution	0.2 K RMS (1.0 s integration time)
Optical resolution	HPBW: 6.0° (Sidelobe level <-30 dBc)
Absolute system stability	1.0 K
Receiver and antenna thermal stabilization	Accuracy <0.05 K
Pointing speed	Elevation: 3°/sec, azimuth: 5°/sec
Radiometric range	0-350 K
Operating temperature range	-40°C to +45°C
Power consumption	<350 watts on average, 500-watt peak
Weight	105 kg for receiver modules, 300 kg for positioner

177

178   Currently, the RPG-4CH-DP provides only the basic brightness temperature (Tb)

179   data in 4 channels without other related products. By incorporating the auxiliary

180   observations from the observation system, we broadened the application of the

181   instrument, denoted RPG-XCH-DP, thereby providing not only the basic microwave

182   radiance but also the complex surface emissivity.

183   **2.2 Mobile system (platform)**

184   The multitarget mobile system comprises a track, a mobile platform, a driving

185   system and a control unit. As the sketch of the mobile system in Fig. 2 shows, the 25

186   m track is parallel to the test plots with an observation interval of 0.3 m. The mobile

187   platform placed on the track is a metal box 4 m in length, 0.8 m in height, and 1.0 m

188   in depth. The driving system includes a stepper motor, transmission mechanism, and

189   communication cable connected to the mobile platform and power supply. The control

190   unit consists of a single-chip microcomputer, timer and stepper motor driver, which

191   can set the moving time and control the operation of the driving device. The control

192   device is installed on the mobile platform and connects both driving devices.

193   In this experiment, to obtain the microwave emissivity over different surfaces in

194   near-simultaneous time, the RPG-4CH-DP is mounted on the mobile platform and

195   moves back and forth along the track. The communication system for receiving the

196 data and the power supply are placed in the metal box. According to the commands

197 from the single-chip microcomputer and the driving force from the stepper motor, the

198 mobile platform moves along the track similar to a small train, and the onboard

199 radiometer scans the 5 test plots at fixed times every day.
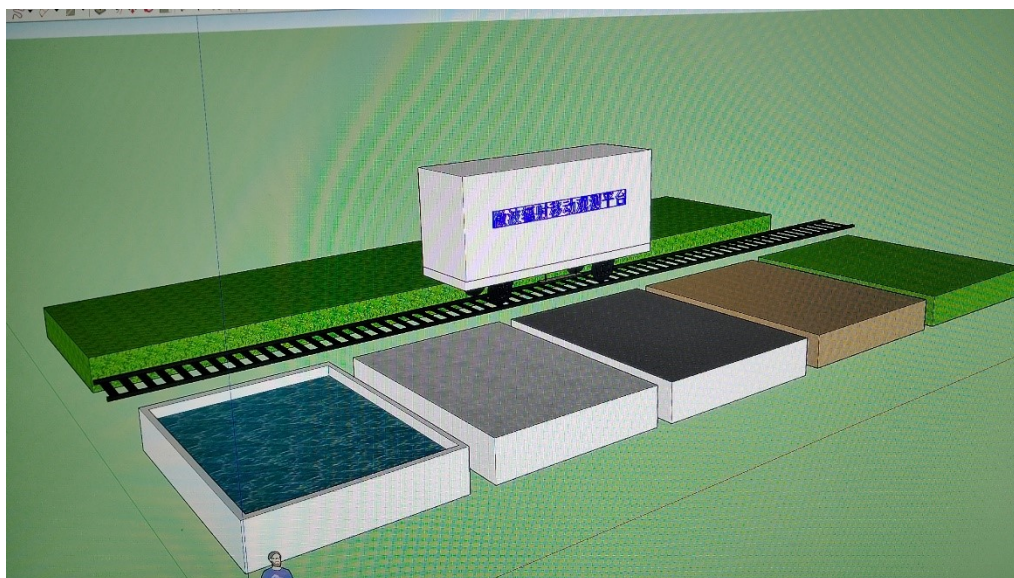
200

201 Fig. 2 Sketch of the mobile platform

2.3 Observation field and auxiliary data

203 Fig. 3 shows a sketch of the observation field, including the 5 test plots

204 distributed along the 25 m track. Currently, 5 surface types are considered in the

205 observation field, namely, water, cement, sand, soil and grass. For the water body, a

206 plastic pool 6 m long and 2.4 m wide is used to hold the water. The adjacent cement

207 surface consists of a 2 m wide footpath. The remaining three plots of sand, bare soil

208 and grass are the same size (approximately 6 m long by 4 m wide) and are separated

209 by a distance of approximately 2 m.
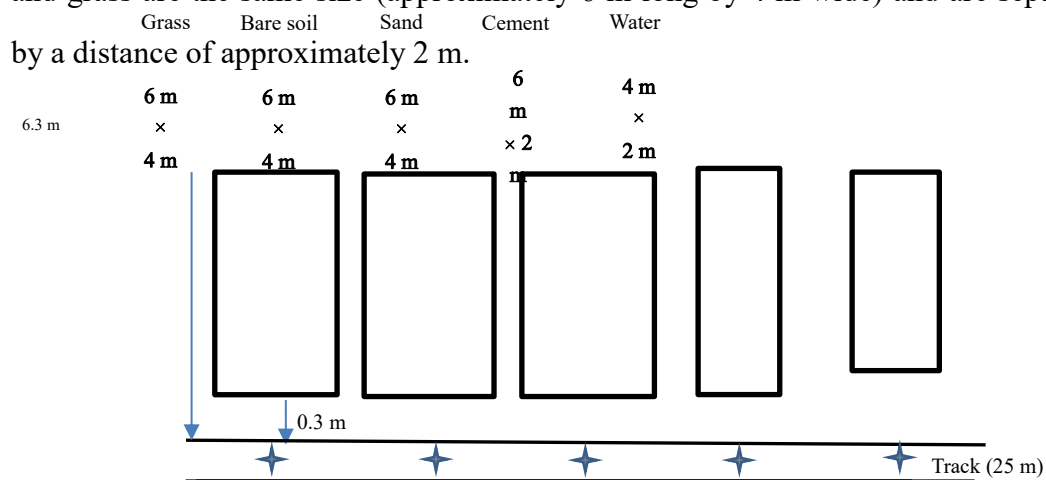
Fig. 3 Sketch of the observation field (including 5 test plots: water, cement, sand, bare soil and grass), where ✦ denotes the position of a touching switch

To scan each plot at the same place at a fixed time, five touching switches corresponding to the center of each plot are fixed on the track to stop the moving platform so that the radiometer can scan the same place for a couple of minutes. By using this mobile platform, the ground-based radiometer can scan multiple surfaces almost simultaneously (i.e., within 1 hr), thereby providing valuable measurements for understanding the variation in surface emissivity over different land surfaces with different characteristics.

The auxiliary data include mainly the surface temperature, soil temperature and soil moisture. Five thermometers with a PT100 temperature sensor made by Honeywell company are placed separately on each test plot to measure their surface temperature. In addition, an SI-111 precision infrared radiometer developed by Apogee Instruments Inc. is fixed on a stand of the RPG-4CH-DP radiometer to obtain the surface temperature of each plot while the microwave radiometer is moving. Furthermore, a set of soil temperature and moisture sensors is fixed at three soil depths, 5 cm, 10 cm and 20 cm, to detect the subsurface soil temperature and humidity. To monitor the real-time working situation of the whole observation system, a digital video camera is installed near the field to record the states of the mobile platform and radiometer as well as changes in the weather, such as the presence of cloud cover, rain or snow.

2.4 Scanning mode

To directly obtain the surface emissivity, a combined mode of ground observations at multiple elevation angles and zenith observations is designed, in which the former monitors mainly the surface radiance while the latter monitors the sky radiance in the same 1 hr period.

The ground observation mode is illustrated in Fig. 4. The mobile platform is triggered every hour, and the microwave radiometer operates using the ground scanning mode at this time. The scan is performed from the horizon (0°) to the ground, and the elevation angle is defined as the angle between the scanning direction and the

248   horizontal. A negative value indicates an angle below the horizon, which is equivalent

249   to 90°-θ, where θ is the incident angle, an important parameter for describing

250   spaceborne radiometer scanning. The radiometer is 2.5 m above the ground, so it can
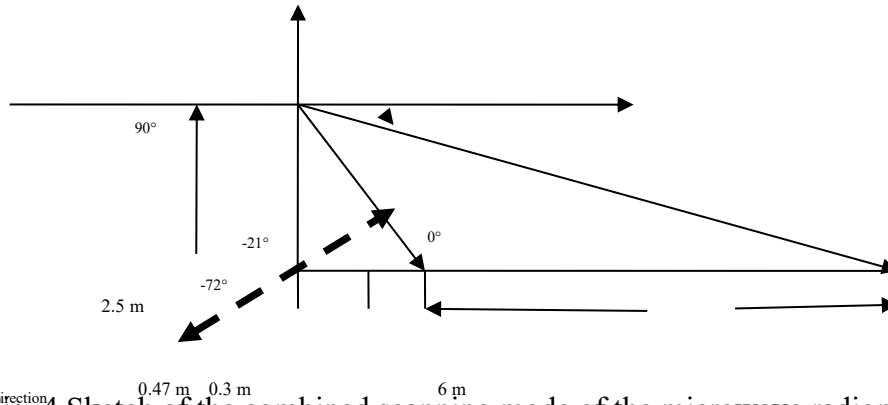
251

252   Fig. 4 Sketch of the combined scanning mode of the microwave radiometer

253

254   scan each test plot with a length of 6 m when the elevation angle is between -21° and

255   -72°, as shown in Fig. 4. The valid elevation angle range for water is different due to

256   the different length of the pool. To determine the surface emissivity variation with the

257   elevation angle, the radiometer is set to scan each test plot with an angle interval of 3°

258   from -21° to -45°, an angle interval of 5° from -45° to -70°, and then back to -21° to

259   scan the test plot repeatedly during the ground observation mode. To acquire ground

260   observations over all 5 test plots within 1 hr, each plot is given 9 minutes; in other

261   words, the mobile platform will move to the cement plot at 9 min, the sand plot at 18

262   min, the bare soil plot at 27 min, and finally the grass plot at 36 min. After finishing

263   the ground observations in all 5 test plots, the mobile platform will begin to move

264   back at 45 min and reach the beginning location after approximately 6 min. During

265   the return trip, the scan mode changes to the zenith observation mode so that the

266   radiometer scans from the ground to the sky. When the elevation angle is raised to 90°,

267   the radiometer will continually acquire zenith observations for approximately 5 min to

268   obtain the sky radiance. After obtaining these zenith observations, the elevation angle

269   changes from the zenith observation mode to the ground observation mode at -21° so

270   that the radiometer is already in the ground observation mode when the next

271 measurement cycle arrives. In this way, the radiometer on the mobile platform can

272 obtain not only the ground radiance over 5 test plots but also the sky radiance within a

273 1 hr period. Here, we assume that 1 hr is short enough to neglect the minute-scale

274 differences in the surface and sky radiance, and thus, the mobile system can obtain the

275 microwave emissivity over different surfaces nearly simultaneously.

276

277 **3 Data and method**

278 Three types of observation data are obtained from the field experiment: the

279 microwave brightness temperature (Tb) at different scanning angles from the ground

280 microwave radiometer; the surface temperature (Ts) of the five test plots measured

281 from the ground thermometers and infrared sensor; and the soil temperature and

282 moisture at three depths in the sand and bare soil plots.

283 When ground microwave radiometer scans the surface, the measured Tb comes

284 mainly from two contributions: that of upward radiation from the surface and that of

285 the reflected downward atmospheric radiance. Thus, the measured Tb can be

286 approximately expressed by Eq. (1):

287 $\qquad T_b = \varepsilon T_s + (1- \varepsilon) T_{sky}$ $\qquad\qquad$ (1)

288 where ε is the surface emissivity, T_s is the surface temperature, and T_{sky} is the radiance

289 from the sky. From Eq. (1), the surface emissivity can be directly calculated using Eq.

290 (2) by combining the Tb contributions from the surface and sky with the surface

291 temperature synchronously measured from the infrared sensor in the observation

292 system.

293 $\qquad \varepsilon = (T_b - T_{sky})/(T_s - T_{sky})$ $\qquad\qquad$ (2)

294 It is noted here that Eq.(1) is assumed for specular reflection, and was used in

295 previous similar observation study (Lemmetyinen et al., 2015; Montpetit et al., 2018),

296 so we used Eq.(1) and (2) to calculate surface emissivity in this work. The

297 dual-polarized radiometer can provide both vertical and horizonal polarization

298 information, then the idea and uniform Lambertian surface is too simple and the

299 bidirectional reflectance (BRDF) surface seems more complex, and the specular

300 reflection is a good option. The results derived from this assumption will be further

301 investigated by combining more auxiliary observations in the actual surface of test plots.

302   Through applying the ground mobile observation system for surface microwave

303 emissivity and combining the video camera records with the soil temperature and

304 moisture measurements, we can not only directly obtain highly accurate surface

305 microwave emissivity observations over different test plots but also investigate the

306 variation characteristics of the surface emissivity under different weather conditions.

307

4. Preliminary results

308

309   Considering both the viewing field of the microwave radiometer and the size of the

310 test plots, the elevation angle range between -24° and -65° is chosen for observing the

311 land test plots (cement, sand, soil and grass), while elevation angles between -33° and

312 -65° are valid for observing the water surface. Here, we focus on the variations in the

313 radiance and surface emissivity over the 5 test plots during the observations recorded

314 in October 2018 under clear sky conditions.

4.1 Radiance

315

316   Since a scanning angle of 36° is equivalent to an incident angle of 54° used for

317 many spaceborne microwave imagers, such as AMSR-E (55°) or SSM/I (53°), we first

318 compare the variation in the observed Tb over different surfaces at an elevation angle

319 of 36°. As Fig.5a shown, the changes in the observed Tb at 36.5 GHz in horizontal

320 (Tb36h) and vertical (Tb36v) polarization over the four land surfaces within 24 hr

321 (Beijing Time, BJT) are quite similar, with smaller values at night and larger values at

322 noon. Less variation in the radiance is noted at Tb36v (not shown), but more

323 significant variations are detected at Tb36h over the four surfaces (Fig. 5a): the

324   observed Tb36h from grass is approximately 270-285 K but varies within 240-270 K

325   over sand and bare soil and reaches only 200-230 K for cement. The observed Tb at

326   18.75 GHz within 24 h shows similar variations with only slight changes among the

327   different land surfaces. Likewise, the corresponding polarization differences (V-H) of

328   Tb within 24 hr are very similar to one another, so both DTb18vh and DTb36vh at

329   02:00 (BJT) are shown in Fig. 5b, revealing a slight difference (close to zero) for

330   grass but considerably larger differences for water and cement (almost up to 70 K for

331   water) and smaller differences over sand and soil (below 30 K). In addition, the values

332   of DTb18vh are larger than those of DTb36vh. The Tb polarization difference is more

333   significant over water than over land and is closely related to the roughness of the

334   land surface. In addition, the roughness of grass is obviously larger than that of the

335   other three land surfaces and thus scatters more surface radiance and reduces the

336   polarization difference. Therefore, the observed Tb polarization differences over the

337   different surfaces shown in Fig. 5b appear reasonable, and the given quantitative

338   polarization differences for certain surfaces can serve as a valid reference for

339   identifying land surfaces and water bodies.
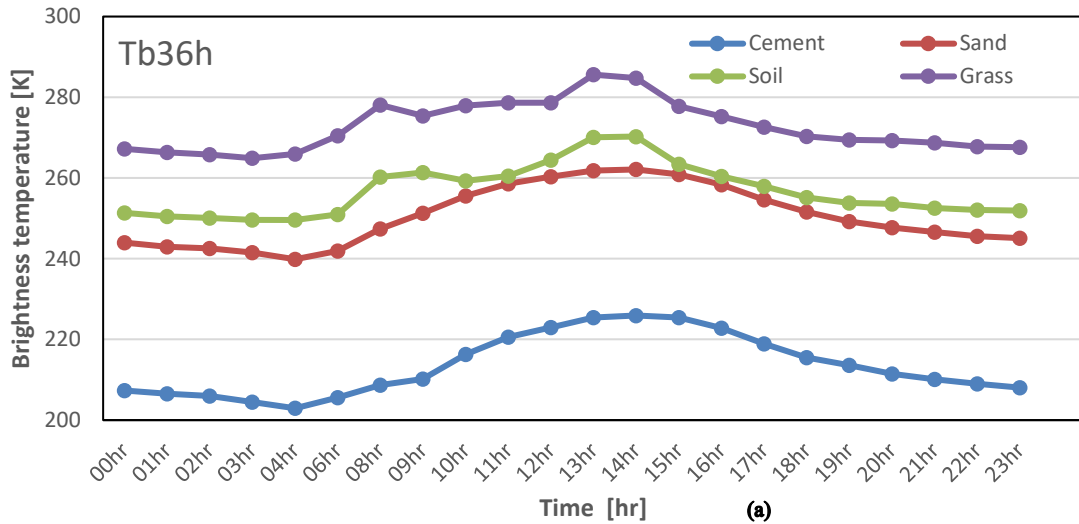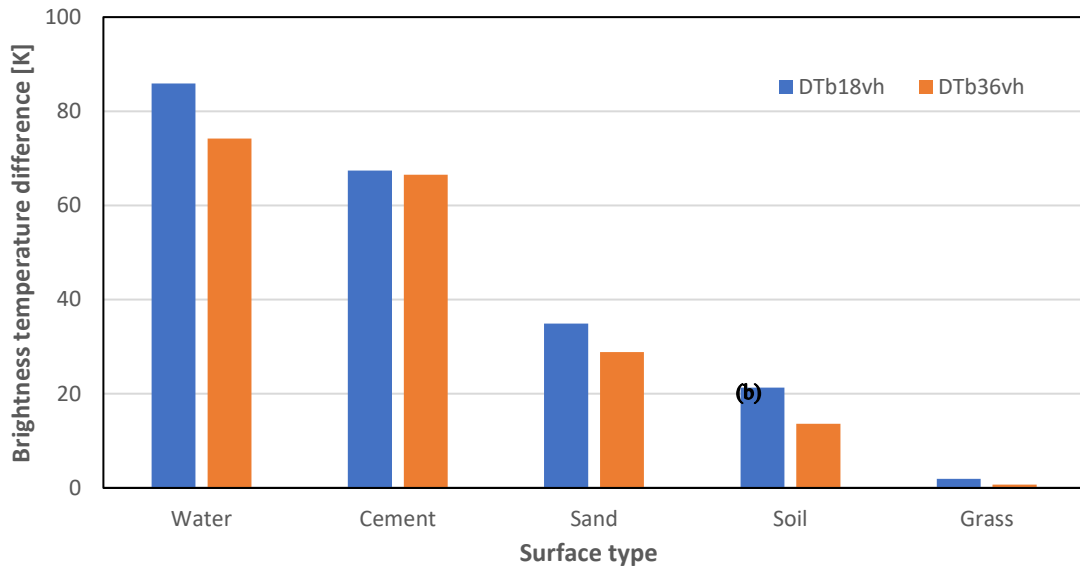
Fig. 5 Variations in the observed Tb (a) and Tb polarization differences (b) over

different surfaces in October 2018.

To study the variations in Tb at more than a single angle, Fig. 6a shows the

changes in the observed Tb with the elevation angle ranging from 24° to 65° over the

four land surfaces. The horizontally polarized Tb is clearly more sensitive to the land

surface type than the vertically polarized Tb with increasing elevation angle; in

particular, Tb36h rises rapidly from 180 K to 240 K over cement but slowly increases

from 240 K to 260 K over sand and bare soil and remains almost constant over grass.

350   In contrast, the variations in the vertically polarized Tb with increasing elevation

351   angle are similar among the land surfaces and are smaller than those in the

352   horizontally polarized Tb, showing a decreasing trend from 280 K to 260 K over

353   different surfaces. The variations in the observed Tb over water are presented in Fig.

354   6b. Different from the above observations over land surfaces, the vertically polarized

355   Tb over water obviously reduces from 200 K to 140 K with increasing elevation angle,

356   while the horizontally polarized Tb slowly rises from 100 K to 120 K, almost opposite

357   to the Tb polarization variations over land surfaces. The corresponding changes in the

358   polarization difference of Tb at 18.75 GHz (DTb18vh=Tb18v-Tb18h) over all 5

359   classes of surfaces are further plotted in Fig. 6c. In general, the Tb polarization

360   difference decreases with increasing elevation angle, and the variated ranges with the

361   elevation angle over the 5 classes surfaces in Fig. 6c are similar to those in Fig.5b;

362   thus, the decreasing trend is most obvious over water and cement and lest evident

363   over grass with increasing elevation angle. The variations of the Tb polarization

364   difference at 36.5 GHz with the elevation angle are similar to those at 18.75 GHz over

365   all 5 test plots.
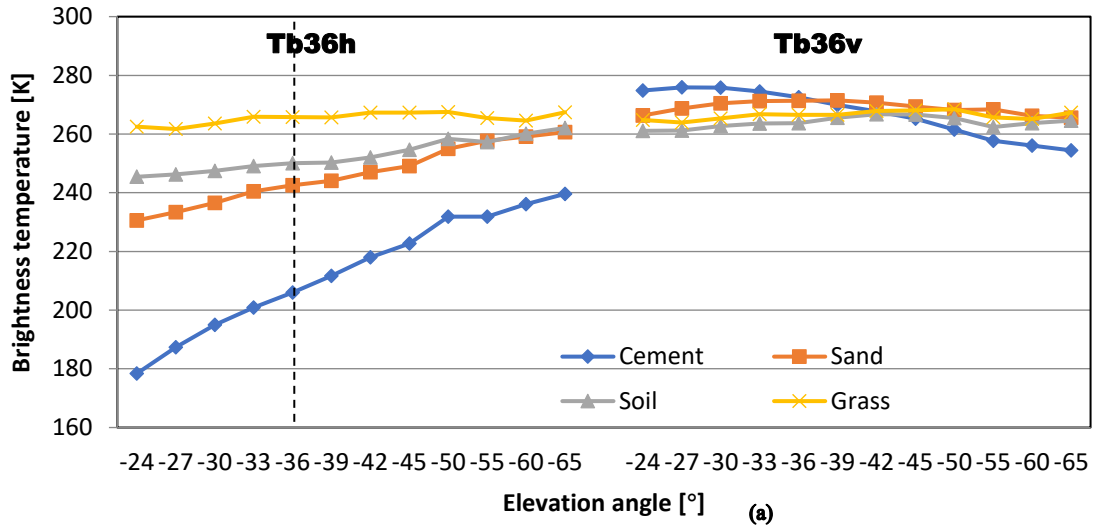
366
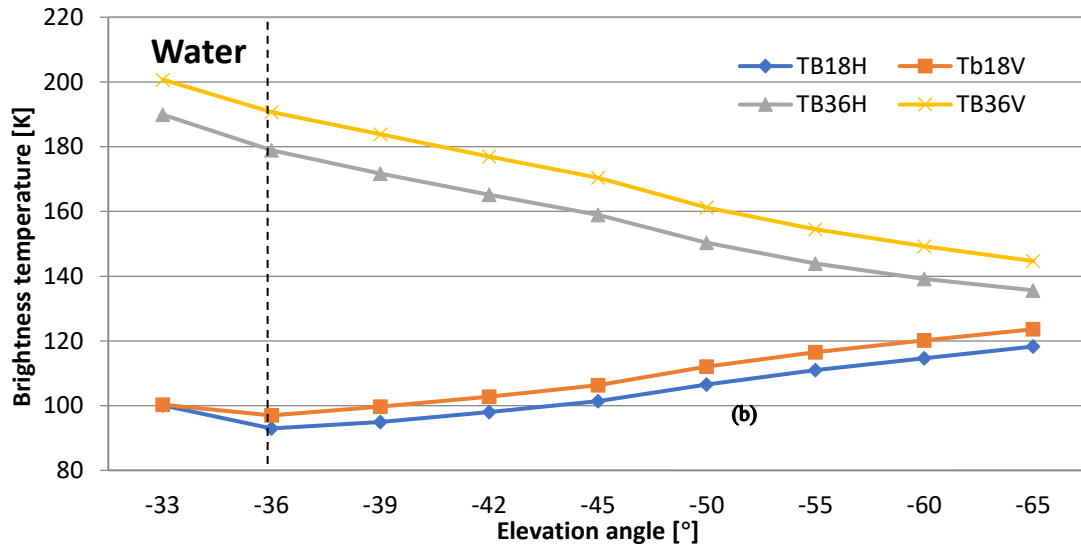
367
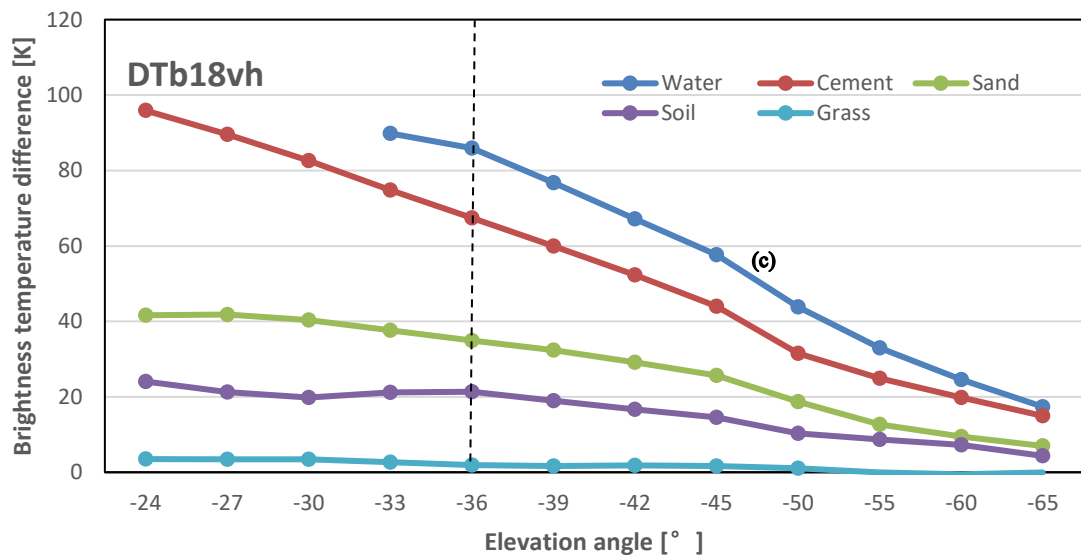
368

369   Fig. 6 Variations in the observed Tb over different land surfaces(a) and water

370   surface(b) as well as Tb polarized difference(c) with the elevation angle. The vertical

371   dotted line corresponding elevation angle 36°

372   **4.2 Surface microwave emissivity**

373   Combining the surface and sky Tb radiance with the surface temperature

374   derived from the infrared sensor, the surface emissivity (ε) is derived from Eq. (2).

375   Since the diurnal variation of ε is more constant and less significant than that of the

376   Tb radiance, the surface emissivity observed at 02:00 (BJT) is chosen for the

377   following investigation. First, the polarized ε at both 18.75 and 36.5 GHz and their

378   polarization differences at an elevation angle of 36° are compared in Fig. 7a. The

379   vertically polarized ε (ε_v) is clearly much larger than the horizontally polarized ε (ε_h),

380   and the ε values at the same frequencies are close, but the ε values over water is

381   smaller than those over the four land surfaces due to quite different dielectric constant.

382   The ε_h values obviously differ among the 4 land surfaces, although their

383   corresponding ε_v values are relatively similar, exceeding 0.95, which indicates that ε_h

384   is more sensitive to land surface variability than ε_v. The ε_h is lower than 0.75 over

385   cement but increases to 0.90 over sand and bare soil and up to 0.97 over grass. Thus,

386   the emissivity polarization difference (ε_v-ε_h) shown in Fig. 7b is obvious over water

387   (>0.3) and cement (approximately 0.25) but reduces to 0.1 over sand and 0.05 over

388   bare soil and almost 0.01 or close to zero over grass; this trend is similar to that of the

389   Tb polarization difference shown in Fig. 5b. Emissivity polarization differences is

390   more significant over water than over land due to different surface reflectivity and

391   dielectric constant property. Among four land surfaces ε_v-ε_h over cement is most

392   obvious and over grass is slight, which is closely related to land surface roughness.

393   Both Tb and emissivity polarized difference demonstrated that surface roughness over

394   grass is obviously larger than that over other three land surfaces, especially smooth

395   cement surface, thus scatters more surface radiance and weakens the polarization

396   difference over grass.
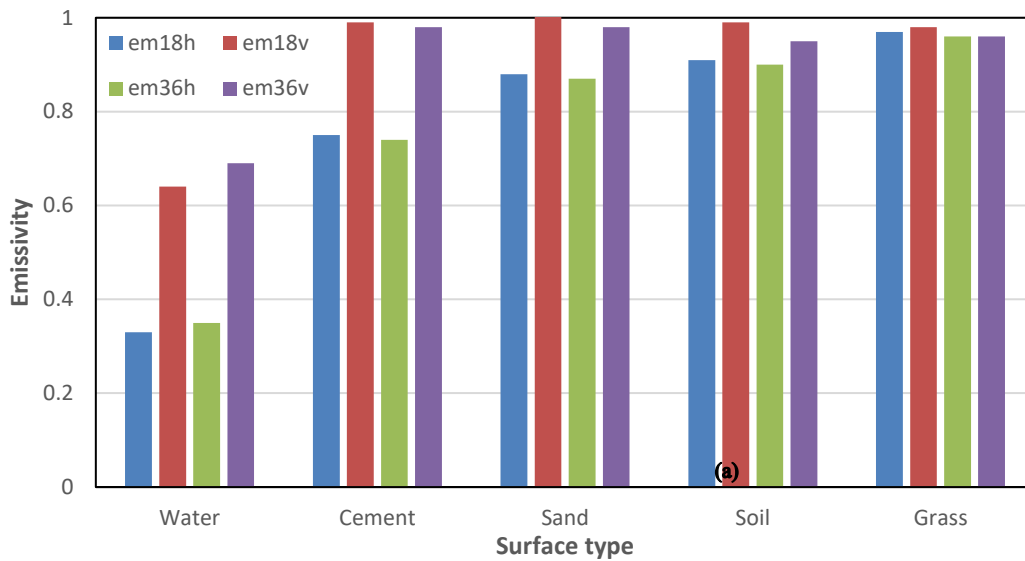
397
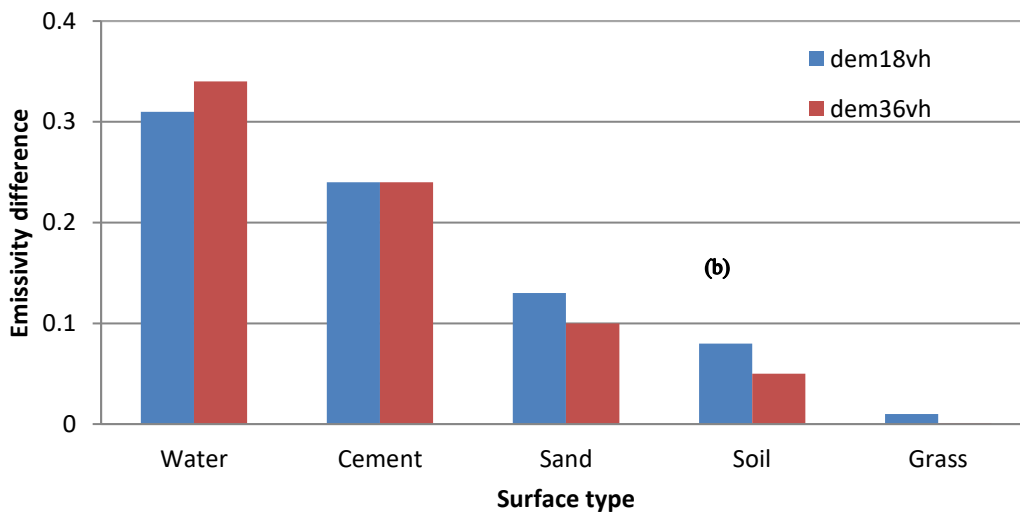
398

399   Fig. 7 Variations in the surface emissivity(a) and emissivity polarization

400   differences (b) over different land surfaces at 02:00 (BJT) in Oct. 2018

401   In addition to investigating the variations at a fixed angle, the variations in ε at

402   multiple elevation angles over the 4 land surfaces are compared in Fig. 8a. Because ε_h

403   is more sensitive to surface type than to water, when the elevation angle changes from

404   -24° to 65°, ε_h clearly rises from 0.65 to 0.85 over cement, followed by sand and bare

405   soil with ε_h increasing from 0.85 to 0.95, and ε_h is constant at 0.95 over grass. The

406   corresponding ε_v values over the four land surfaces are closer and exhibit a slightly

407   decreasing trend within the range of 0.9-1.0 with increasing elevation angle.

408

409

410
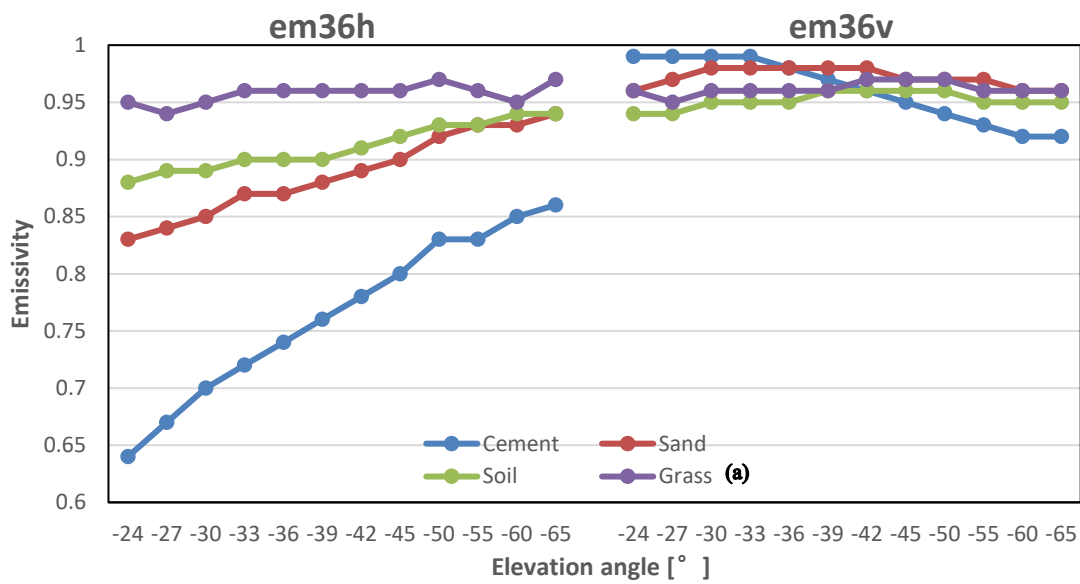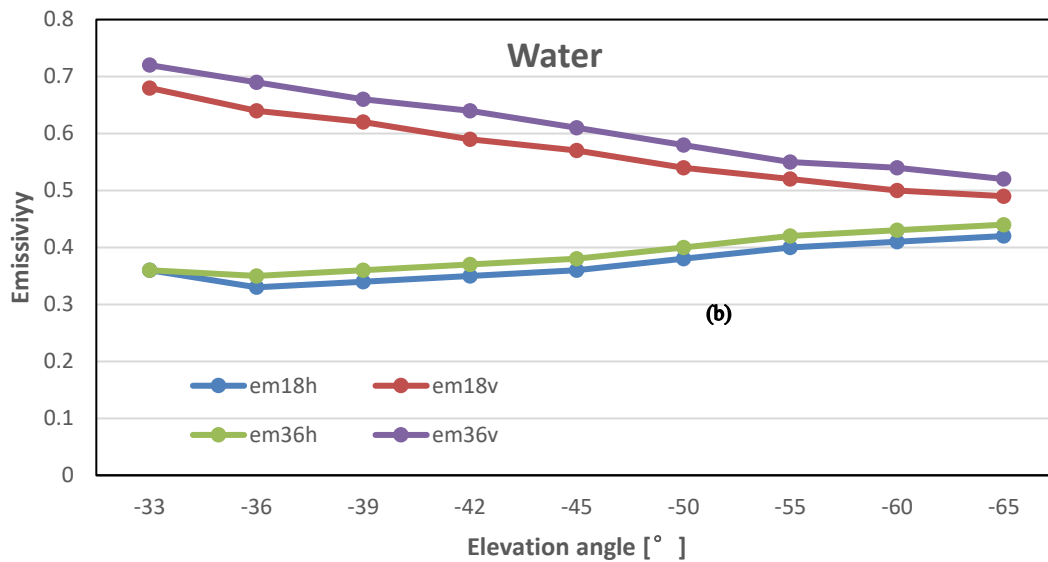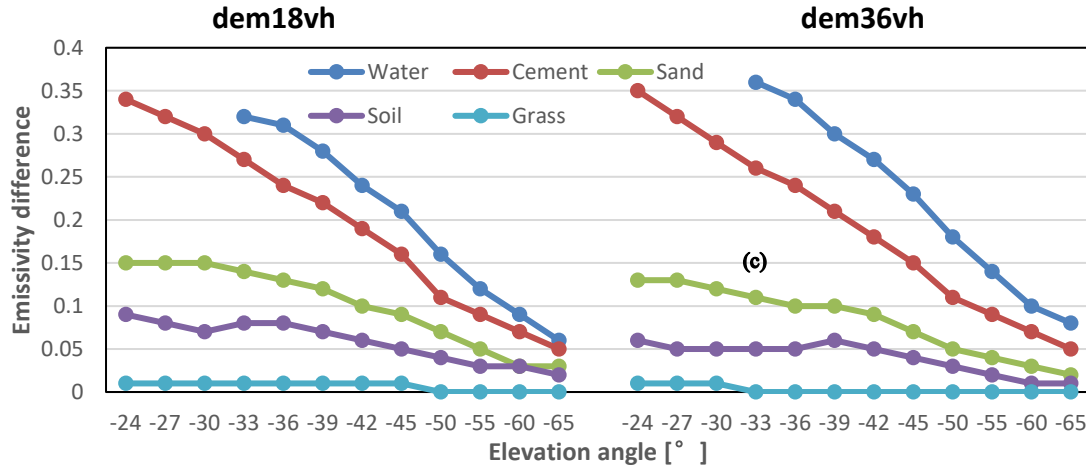
Fig. 8 Variations in the surface emissivity (a, b) and ε polarization

differences(c) over different surfaces with increasing elevation angle.

Differ from land surfaces, the ε values over water in Fig. 8b show considerably

different variation trends with the elevation angle: when the elevation angle changes

from -33° to -65°, ε_v clearly reduces from 0.7 to 0.5, while ε_h slightly increases within

the vicinity of 0.4. The corresponding ε polarization differences (ε_v-ε_h) over 5 surfaces

(Fig. 8c) present decreasing trend with increasing elevation angle, and the larger the ε

polarization difference in Fig. 7b is, the greater the variation with the elevation angle

in Fig. 8c is, i.e. the decreasing trend is most obvious over water and smooth cement,

but slightly changes over grass with increasing elevation angle. The variation in the ε

polarization difference at 36.5 GHz with the elevation angle is similar to that at 18.75

GHz over all 5 test plots (results not shown).

5 Summary

In this paper, we introduce a ground mobile observation system for directly

obtaining surface microwave emissivity estimates over five types of surfaces: water,

cement, sand, soil and grass. The mobile observation system consists mainly of a

427   dual-polarized ground-based microwave radiometer, a mobile platform, and auxiliary

428   sensors, and the observation field comprises 5 test plots.

429   Based on the observed data from the mobile system, we preliminarily

430   investigated the variation characteristics of the surface microwave emissivity over the

431   five different land surfaces. The results show that the horizontally polarized

432   emissivity is more sensitive to land surfaces type than is the vertically polarized

433   emissivity: the former decreases to 0.75 over cement and increases to 0.90 over sand

434   and bare soil and up to 0.97 over grass. The observed polarization difference is

435   obvious over water (>0.3) and cement (approximately 0.25) but reduces to 0.1 over

436   sand and 0.05 over bare soil and almost 0.01 or close to zero over grass; this trend is

437   similar to that of the Tb polarization difference. For different elevation angles, the

438   horizontally/vertically polarized emissivities over the land surfaces obviously

439   increase/slightly decrease with increasing elevation angle but exhibit the opposite

440   trend over water. The emissivity polarization difference decreases with increasing

441   elevation angle, and the larger the emissivity polarization difference is over a certain

442   surface, the greater the variation with the elevation angle.

443   We developed a ground mobile observation system for measuring the microwave

444   emissivity over multiple surfaces, and the system has worked stably since September

445   2018. The preliminary results from our observation system partly reflect similar

446   variation trends to those reported by previous surface emissivity experiments, and

447   some are more related to the variation in emissivity at different elevation angles. In

448   future research, we will carry out further analyses and refine the emissivity

449   parameterization scheme for given surfaces based on long-term observations.

450

451   **Acknowledgments**

452   This work was supported by National Natural Science Foundation of China [No.

453   41575033] and National Key Research and Development Program of China

454   [2017YFC1501700]. We thank the staffs at Xianghe site for their maintenance work

455   on microwave radiometer and the ground mobile observation system.

456

457   References

458   Calvet, J. C., Wigneron J. P., Chanzy. A.,Raju S., and Laguerre L.: Microwave dielectric
459   proporeties of a silt-loam at high frequencies, IEEE Trans. Geosci. Remote sensing, 33,
460   634-642,doi: 10.1109/36.387579, 1995.

461   Fung A. K.: Microwave Scattering and Emission Models and Their Applications. Norwood, MA:
462   Artech House, 1994.

463   Karbou, F., Aires F., Prigent C., and Eymard L.: Potential of Advanced Microwave Sounding Unit-A
464   (AMSU-A) and AMSU-B measurements for atmospheric temperature and humidity profiling over
465   land, Journal of Geophysical Research, 110, D07109, doi:10.1029/2004JD005318, 2005.

466   Hewison T. J.: Airborne measurements of forest and agricultural land surface emissivity at
467   millimeter wavelengths. IEEE Trans. Geosci. Remote sensing., 39, 393-400,
468   DOI:10.1109/36.905247, 2001.

469   Hewison, T. J., and English S. J.: Airborne retrievals of snow and ice surface emissivity at
470   millimeter wavelengths. *IEEE Trans. Geosci. Remote Sens.*, 37, 1871-1887,
471   doi:10.1109/36.774700,1999.

472   Isaacs R. G., Jin Y. Q., Worsham R. D., Deblonde, G., Falcone, V. J.: The RADTRAN microwave
473   surface emission models. IEEE Trans.Geosci. Remote sensing, 27, 433-440,
474   DOI:10.1109/36.29563,1989.

475   Jones, A.S., Vonder Haar, T.H.: Retrieval of microwave surface emittance over land using
476   coincident microwave and infrared satellite measurements,*J. Geophys. Res.*,102,13,609-13,626,
477   https://doi.org/10.1029/97JD00797,1997.

478   Lemmetyinen, J., Derksen C., Toose, P., Proksch,C., Pulliainen, J., Kontu, A., Rautiainen, K.,
479   Seppänen, J., Hallikainen, M.: Simulating seasonally and spatially varying snow cover brightness
480   temperature using HUT snow emission model and retrieval of a microwave effective grain size,
481   Remote Sens. Environ.,156,71-95, http://dx.doi.org/10.1016/j.rse.2014.09.016,2015.

482   Mazler C.: Seasonal evolution of microwave radiation from an oat field, Remote Sens. Environ., 31,
483   161-173, doi:10.1016/0034-4257(90)90086-2,1990.

484   Mazler C.: Passive microwave signatures of landscapes in winter, Meteorol. Atmos. Phys., 54,
485   241-260, https://doi.org/10.1007/BF01030063, 1994.

486   McNally A. P., Derber J. C., Wu W. S., Katz, B.B.: The use of TOVS level-1B radiances in the
487   NCEP SSI analysis system, Quarterly Journal of the Royal Meteorological Society, 126, 689-724,
488   https://doi.org/10.1002/qj.49712656315, 2000.

Mo, T., Schmugge, T.J.: A parameterization of the effect of surface roughness on microwave emission, IEEE Trans. Geosci. Remote Sens., 4, 481–486, **doi:** 10.1109/TGRS.1987.289860, 1987.

Moncet, J.L., P. Liang, J. F., Galantowicz, et al., 2011: Land surface microwave emissivities derived from AMSR-E and MODIS measurements with advanced quality control. *J. Geophys. Res.*, 116, D16104, doi:10.1029/2010JD015429.

Montpetit, B., Royer, A., Roy, A., Langlois, A.: In-situ passive microwave emission model parameterization of sub-arctic frozen organic soils, Remote Sens. Environ.,205,112-118, https://doi.org/10.1016/j.rse.2017.10.033,2018.

Morland, J. C., Grimes D.I.F., Dugdale, G., Hewison, T.J.: The Estimation of Land Surface Emissivities at 24 GHz to 157 GHz Using Remotely Sensed Aircraft Data, Remote Sens. Environ., 73, 323-336, https://doi.org/10.1016/S0034-4257(00)00108-5,2000.

Morland, J. C., Metcalfe J., and Walker A.: Microwave remote sensing of soil moisture in southern Ontario: Aircraft and satellite measurements at 19 and 37 GHz, Radio Sci., 38, 8073, doi:10.1029/2002RS002677, 2003.

Njoku, E.G., and O'Neill P. E.: Multifrequency microwave radiometer measurements of soil moisture, IEEE Trans. *Geosc. Remote Sens.,* 20, 468-475, doi:10.1109/TGRS.1982.350412, 1982.

Ruston R. C., Vonder Haar T. H.: Characterization of summertime microwave emissivity from the Special Sensor Microwave Imager over the conterminous United States, J. Geophys. Res., 109, D19103, doi:10.1029/2004JD004890, 2004.

Prigent,C., Rossow, W.B., Matthews, E.:Microwave land surface emissivities estimated from SSM/I observations, *J. Geophys. Res.*,102, 21867-21890, https://doi.org/10.1029/97JD01360,1997.

Prigent, C., Rossow, W. B., Matthews, E., and Marticorena, B.: Microwave radiometric signatures of different surface types in deserts, *Journal of Geophysical Research*, 104, 12147-12158, doi: 10.1029/1999JD900153, doi:10.1029/1999JD900153, 1999.

Prigent, C., Wigneron, J. P., Rossow, W. B., and Pardo-Carrionet, J.R.: Frequency and angular variations of land surface microwave emissivities: Can we estimate SSM/T and AMSU emissivities from SSM/I emissivities? IEEE Trans.Geosci. Remote sensing, 38, 2373-2386, doi:10.1109/36.868893, 2000.

Prigent, C., Aires F., and Rossow W. B.: Land surface microwave emissivities over the globe for a decade, Bull. Amer. Meteorol. Soc., **87**, 1573 - 1584, https://doi.org/10.1175/BAMS-87-11-1573, 2006.

Schwartz, C. S., Liu, Z. Q., Chen, Y., Huang, X.Y.: Impact of assimilating microwave radiances with a limited-area ensemble data assimilation system on forecasts of Typhoon Morakot, Weather Forecasting, 27, 424-437, https://doi.org/10.1175/WAF-D-11-00033.1,2012.

Ulaby, F. T., Moore, R. K., Fung, A. K.: Microwave Remote Sensing: Active and Passive. Vol. 3: From Theory Applications. Addison-Wesley Publ. Company, Readings, Massachusettes, 1986.

Wang, J. R. and Choudhury, B. J.: Remote sensing of soil moisture content over bare field at 1.4 GHz frequency, J. Geophys. Res., 86, 5277–5282, 1981.

Wigneron, J. P., Guyon, D., Calvet, J. C., Courrieer G., Bruguier N.: Monitoring coniferous forest characteristics using a multifrequency microwave radiometry, Remote Sens. Environ., 60, 299-310, doi:10.1016/S0034-4257(96)00212-X,1997.

Weng, F., Yan, B., Grody N.C.: A microwave land emissivity model, J. Geophys. Res., 106, 20,115-20,123, https://doi.org/10.1029/2001JD900019, 2001.

533   Xie, Y., Shi, J., Ji, D., Zhong, J., Fan, S.:A Parameterized Microwave Emissivity Model for Bare

534   Soil Surfaces,Remote sensing, 9, 155-170, https://doi.org/10.3390/rs9020155, 2017.